Journal of Advances in Modeling Earth Systems

RESEARCH ARTICLE
10.1029/2018MS001476

Key Points:
- Simulations at forest sites exhibit nocturnal low bias of temperature and friction velocity, midday high bias of sensible heat
- Inclusion of biomass heat storage parameterization reduces these biases concurrently
- The parameterization shows similar positive impact across multiple sites with different plant functional types and climates

Correspondence to:
S. Swenson,
swensosc@ucar.edu

Citation:
Swenson S., Burns, S. P., & Lawrence, D. M. (2019). The impact of biomass heat storage on the canopy energy balance and atmospheric stability in the community land model, *Journal of Advances in Modeling Earth Systems*, *11*, 83–98. https://doi.org/10.1029/2018MS001476

Received 15 AUG 2018
Accepted 12 DEC 2018
Accepted article online 17 DEC 2018
Published online 15 JAN 2019

©2018. The Authors.
This is an open access article under the terms of the Creative Commons Attribution-NonCommercial-NoDerivs License, which permits use and distribution in any medium, provided the original work is properly cited, the use is non-commercial and no modifications or adaptations are made.

The Impact of Biomass Heat Storage on the Canopy Energy Balance and Atmospheric Stability in the Community Land Model

Sean C. Swenson[1], **Sean P. Burns**[1,2], **and David M. Lawrence**[1]

[1] National Center for Atmospheric Research, Boulder, CO, USA, [2] Department of Geography, University of Colorado, Boulder, CO, USA

Abstract Atmospheric models used for weather prediction and future climate projections rely on land models to calculate surface boundary conditions. Observations of near-surface states and fluxes made at flux measurement sites provide valuable data with which to assess the quality of simulated lower boundary conditions. A previous assessment of the Community Land Model version 4.5 using data from the Niwot Ridge Subalpine Forest AmeriFlux tower showed that simulated latent heat fluxes could be improved by adjusting a parameter describing the maximum leaf wetted area, but biases in midday sensible heat flux and nighttime momentum flux were generally not reduced by model parameter perturbations. These biases are related to the model's lack of heat storage in vegetation biomass. A biomass heat capacity is parameterized in Community Land Model version 5 with measurable quantities such as canopy height, diameter at breast height, and tree number density. After implementing a parameterization describing the heat transfer between the forest biomass and the canopy air space, the biases in the mean midday sensible heat and mean nighttime momentum fluxes at Niwot Ridge are reduced from 47 to 13 W/m^2 and from 0.12 to −0.03 m/s, respectively. The bias in the mean nighttime canopy air temperature was reduced from −5.9 to 0.4 °C. Additional simulations at other flux tower sites demonstrate a consistent reduction in midday sensible heat flux, a lower ratio of the sum of sensible and latent heat flux to net radiation, and an increase in nighttime canopy temperatures.

Plain Language Summary Community Land Model exhibits a strong nighttime cold bias in surface temperature at forested sites. Representing the heat stored and released by vegetation biomass largely reduces this bias in the model, as well as biases in nighttime friction velocity and midday sensible heat flux.

1. Introduction

The calculation of the exchange of heat, moisture, and momentum from the land to the atmosphere is one of the primary purposes of a land model coupled to an atmospheric model. It is therefore important to assess the ability of a land model to accurately reproduce the observed surface energy budget (Leuning et al., 2012). Burns et al. (2018) used above-canopy eddy-covariance measurements to calculate the warm-season diel cycle of the fluxes of sensible heat, latent heat, and momentum at the Niwot Ridge Subalpine AmeriFlux site. (Note that the term "diel" indicates the full 24-hr cycle, not only daytime [diurnal] but also nighttime [nocturnal] periods). The observed diel cycle composites showed that the Community Land Model version 4.5 (CLM4.5) underestimated the latent heat flux increase following a precipitation event, overestimated midday sensible heat flux, and underestimated nighttime friction velocity (a measure of momentum flux). While changing the model parameter controlling the maximum leaf wetted fraction improved the simulated latent heat flux, the biases of the sensible heat and momentum were not resolved through adjustment of a range of parameters (Burns et al., 2018).

Other land models have also been shown to exhibit significant surface energy flux biases. In the PLUMBER project (Best et al., 2015), the authors defined a set of benchmarks against which they assessed the simulated sensible and latent heat fluxes from 13 land models at 20 sites. Best et al. (2015) found that none of the models performed better at simulating sensible heat flux than a linear regression against incoming shortwave solar radiation. In a subsequent analysis of the PLUMBER simulations, Haughton et al. (2016) tested whether

methodological issues, errors in the observations, or incorrect model structures and process representations could explain the poor model performance with respect to the empirical model. Their analysis cast doubt on the first two explanations, and Haughton et al. (2016) hypothesized that the models might instead share a missing component or relationship between components.

One process that is absent from CLM is the storage of heat within vegetation, and the exchange of that heat with the surrounding canopy air space. In a discussion of the "energy imbalance problem," Leuning et al. (2012) noted that phase lags due to incorrect estimates of energy storage in soils, air, and biomass can explain why the sum of sensible and latent heat rarely matches available energy at flux measurement sites. Using measurements from a research site in Sweden, Lindroth et al. (2010) estimated the storage flux for biomass, canopy air, and soil and found that the heat flux from the tree biomass was the largest of the storage components. Lindroth et al. (2010) also showed that the regression coefficient of 0.86 between the sum of the sensible and latent heat fluxes and net radiation was increased to 0.95 when the biomass storage flux was added to the sensible and latent heat fluxes. Haverd et al. (2007) incorporated a tree trunk heat store in a soil vegetation atmosphere transfer model for a Eucalyptus forest in Australia and were able to balance the available energy with the sum of the sensible and latent heat fluxes to within a percent; at the same time, the agreement between the modeled and measured individual heat fluxes improved.

At the Niwot Ridge tower site, Burns et al. (2015) used thermocouples placed within tree trunks to estimate the tree biomass heat flux. They found that the storage heat fluxes were as much as 15% of daily maximum net radiation. To test whether biomass heat storage (BHS) can help resolve the discrepancy between the observed and simulated surface energy diel cycle at the Niwot Ridge AmeriFlux site (Burns et al., 2018), we modified the CLM version 5 (CLM5) surface energy budget to include the heat stored by vegetation biomass. The canopy is composed of two separate thermal reservoirs, one for leaves and another for stems (i.e., trunks and branches). After comparing the original and the modified CLM simulations to the observations from Niwot Ridge, we perform simulations for other flux towers having different regional climates and vegetation types.

2. Flux Measurement Sites

2.1. Niwot Ridge Subalpine Forest AmeriFlux Site

The Niwot Ridge Subalpine Forest AmeriFlux site (site US-NR1, Blanken et al., (1998–present) is located in the Rocky Mountains of Colorado (40.03°N, 105.55°W) at an elevation of 3,050 m. Soils are typically classified as a loamy sand in dry locations, overlain by roughly 10 cm of organic material. The tree density around the site is about 4,000 trees per hectare with a leaf area index (LAI) of 3.8–4.2 m^2/m^2 and tree heights of 12–13 m. The subalpine forest surrounding the US-NR1 tower was established in the early 1900s following logging operations and is composed of approximately 46% subalpine fir (Abies lasiocarpa var. bifolia), 28% Englemann spruce (Picea engelmannii), and 26% lodgepole pine (Pinus contorta). Observations of meteorological quantities and ecosystem fluxes are made at a height of 21.5 m. More details about US-NR1 can be found in, for example, Monson et al. (2002) and Burns et al. (2015).

2.2. Additional Flux Measurement Sites

To test whether the parameterization developed and validated for US-NR1 performs consistently for other plant functional types (PFTs) and different climate conditions, simulations were run for 11 additional flux measurement sites (Table 2).

3. The CLM

3.1. Model Overview

The CLM (Lawrence et al., 2011) is the land component of the Community Earth System Model (Hurrell et al., 2013). CLM simulates the partitioning of moisture and energy from the atmosphere, the redistribution of moisture and energy within the land surface, and the export of fresh water and heat to the oceans. Biogeophysical processes represented in CLM include solar and longwave radiation interactions with the vegetation canopy and soil; turbulent fluxes of momentum, heat, and moisture from canopy and soil; heat and moisture transfer through soil and snow; and stomatal physiology and photosynthesis. Some of the hydrological processes included are interception of precipitation by the vegetation canopy, throughfall, infiltration into soils, surface and subsurface runoff, snow and soil moisture evolution, evaporation from soil, and vegetation and transpiration (Oleson et al., 2013). CLM is a "big leaf" model, in which the canopy is conceptualized as a single vegetation layer whose interactions with the atmosphere and ground are modulated by the canopy air space (Bonan, 2015; Oleson et al., 2013).

Table 1
Biomass Heat Storage Simulation Parameters

Parameter	Value	Units
D_{bh}	0.2	m
h_{tree}	13	m
N_{tree}	0.4	m^{-2}
f_w	0.45	kg/kg
r_{bole}	200	s/m
ζ_{max}	100	
k_{vert}	0.1	
k_V	1	
k_A	1	

For this study, CLM5 was run with prescribed, satellite-derived phenology in both single-point mode (driven with 30-min flux measurement tower observations) and globally (driven with 3-hourly atmospheric reanalysis-based forcing data). The above-canopy observations used for model input are horizontal wind speed, air temperature, relative humidity, barometric pressure, precipitation, and incoming shortwave and longwave radiation. For the US-NR1 simulations, the CLM soil texture was set to a loamy sand (72% sand, 27% silt, 1% clay; Burns et al., 2018). Soil thickness was specified to be 1.2 m. Canopy height was set to 13 m.

3.2. CLM Canopy Energy Balance

The conservation of energy within the canopy in CLM is obtained by solving for a vegetation temperature that balances the sum of the net radiation absorbed by the canopy with the sensible and latent heat flux from the canopy to the canopy air space (Oleson et al., 2013).

Both the canopy and the air within the canopy are assumed to have a negligible heat capacity. With these assumptions, the canopy energy budget becomes

$$\vec{S}_{veg} + \vec{L}_{veg}\left(T_{veg}\right) - H_{veg}\left(T_{veg}\right) - \lambda E_{veg}\left(T_{veg}\right) = 0, \tag{1}$$

where $\vec{S}_{veg}$ is the solar radiation absorbed by the vegetation (W/m^2), $\vec{L}_{veg}$ is the net longwave radiation absorbed by the vegetation (W/m^2), H_{veg} and λE_{veg} are the sensible and latent heat fluxes from the vegetation (W/m^2), respectively (Oleson et al., 2013). T_{veg} is the vegetation temperature (K) and $\lambda = 2.5\ 10^6$ J/kg is the latent heat of vaporization.

Table 2
Flux Measurement Sites

Number	Site name	Longitude	Latitude	PFT	Time period
1	US-NR1	254.45	40.03	NETe	1998–2007
2	US-UMB	275.29	45.56	BDTe	1999–2006
3	US-Ho1	291.26	45.20	NETe	1996–2004
4	US-MOz	267.81	38.74	BDTe	2004–2007
5	US-WCr	269.92	45.80	BDTe	1998–2006
6	AU-Tum	148.15	−35.65	BETe	2002–2014
7	BR-Sa3	305.03	−3.02	BETr	2001–2003
8	CA-Oas	253.80	53.63	BDBo	1997–2006
9	DE-Tha	13.57	50.96	NETe	1998–2003
10	FL-Hyy	24.29	61.85	NEBo	2005–2014
11	RU-SkP	129.17	62.25	NDBo	2012–2014
12	ZM-Mon	23.25	−15.43	BDTr	2005–2008

Note. PFT Identifiers. Character 1: (N/B) = (Needleleaf/Broadleaf); Character 2: (E/D) = (Evergreen/Deciduous); Characters 3–4: (Bo/Te/Tr) = (Boreal/Temperate/Tropical). PFT = plant functional type.

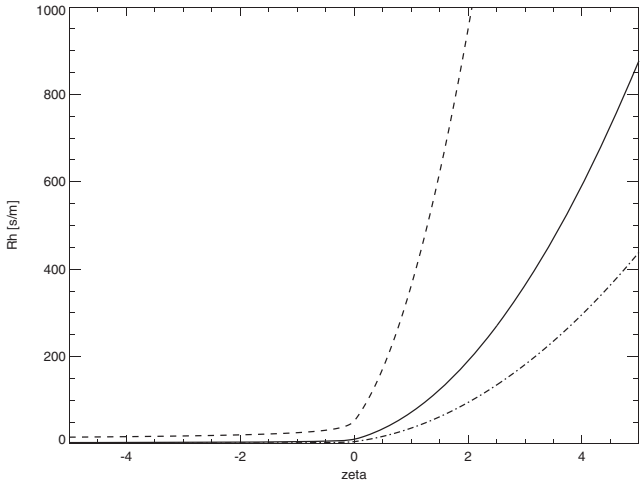

Figure 1. Aerodynamic resistances to sensible heat transfer (s/m) for atmospheric wind speeds of 1 (dashed line), 5 (solid line), and 10 m/s (dot-dashed line) as a function of the Monin-Obukhov similarity theory stability parameter ζ. Negative values of ζ indicate unstable conditions; positive values of ζ indicate stable conditions.

During each model time step, the vegetation temperature is determined by using the iterative Newton-Raphson method to find the root of equation (1). The iteration is ended when either the change in the vegetation temperature falls below a specified tolerance or 40 iterations have been made. Although canopy air temperature is not a prognostic model variable, a diagnostic canopy air temperature is calculated by

$$T_{ca} = \frac{c^h_{atm} T_{atm} + c^h_g T_g + c^h_{veg} T_{veg}}{c^h_{atm} + c^h_g + c^h_{veg}}, \tag{2}$$

where T_{ca} is the canopy air space temperature, T_{atm} is the atmospheric air temperature, T_g is the ground surface temperature, and c^h_{atm}, c^h_g, and c^h_{veg} are the sensible heat conductances (inverse resistances, i.e., $c = \frac{1}{R}$) between the canopy air and the atmosphere, ground, and vegetation, respectively. All temperatures are in units of K, and all conductances are in units of meters per second.

Burns et al. (2018) showed that during the day, T_{ca} was reasonably simulated, but at night T_{ca} was typically 2–5 °C cooler than temperatures measured by thermocouples placed at different heights within the canopy. Also during the night, modeled friction velocity u_* was roughly two thirds of the observed value indicating that the CLM resistances to turbulent exchange were too large. CLM uses Monin-Obukhov similarity theory (Businger et al., 1971; Oleson et al., 2013) to determine the atmospheric resistances to momentum, heat, and moisture based on a dimensionless stability variable ζ. Figure 1 shows the aerodynamic resistance to sensible heat R_h, as a function of ζ, for atmospheric wind speeds of 1, 5, and 10 m/s. Neutral conditions correspond to $\zeta = 0$, unstable conditions (i.e., $T_{ca} > T_{atm}$) correspond to $\zeta < 0$, and stable conditions (i.e., $T_{ca} < T_{atm}$) correspond to $\zeta > 0$. As ζ increases and conditions become more stable, the aerodynamic resistance increases nonlinearly. In CLM4.5, the value of ζ in stable conditions ($\zeta > 0$) was constrained to have a value less than $\zeta_{max} = 2$. Burns et al. (2018) found that by reducing ζ_{max} from 2 to 0.5, the biases in nighttime canopy temperature and friction velocity were reduced, while the overestimation of midday sensible heat flux was not significantly affected. CLM5 uses $\zeta_{max} = 0.5$ as its default value.

4. CLM5 Assessment

4.1. CLM Canopy Temperature Bias

We assess the model with an effective canopy temperature T_{eff} obtained by using the observed upwelling longwave radiation and the surface emissivity used in CLM ($\epsilon = 0.989$) to invert the Stefan-Boltzmann equation for a radiative surface temperature. An example of the nighttime temperature cold bias identified by Burns et al. (2018) is shown in Figure 2 for a week in August 2003; this bias is typical of the model behavior throughout the year. The left panel of Figure 2 shows that during the day, T_{eff} increases relative to T_{atm}, but at night the two temperatures decrease to a similar value. In the right panel of Figure 2, T_{eff} is compared to canopy air temperatures from three CLM simulations that are the same except for the value of ζ_{max}. When the atmospheric stability is effectively unconstrained ($\zeta_{max} = 100$), nighttime canopy temperatures are typically between 5 and 15 °C colder than T_{eff}. As observed by Burns et al. (2018), progressively reducing ζ_{max} brings T_{ca} closer to T_{eff}.

4.2. Atmospheric Stability and Aerodynamic Resistance

The model behavior seen in Figure 2 can be explained by considering equation (1). During the night, insolation is zero and the latent heat flux is small (Burns et al., 2018). Thus, the nighttime canopy energy budget is primarily a balance between net longwave radiation and sensible heat flux between the atmosphere and the canopy. Although T_{atm} and T_{eff} are similar at this time of day, the lower atmospheric emissivity (0.8 vs 0.989) results in a net loss of longwave radiation from the canopy. To conserve energy in CLM, the canopy temperature must decrease until the net longwave loss is balanced by a gain in sensible heat from the atmosphere to the canopy. When the CLM canopy temperature cools below the atmospheric temperature, stable conditions are diagnosed from the Monin-Obukhov stability parameterization. If the stability parameter is unconstrained, a positive feedback occurs in which cooler canopy temperatures lead to larger aerodynamic resistances, further inhibiting sensible heat transfer to the canopy. When resistances become large, which occurs when

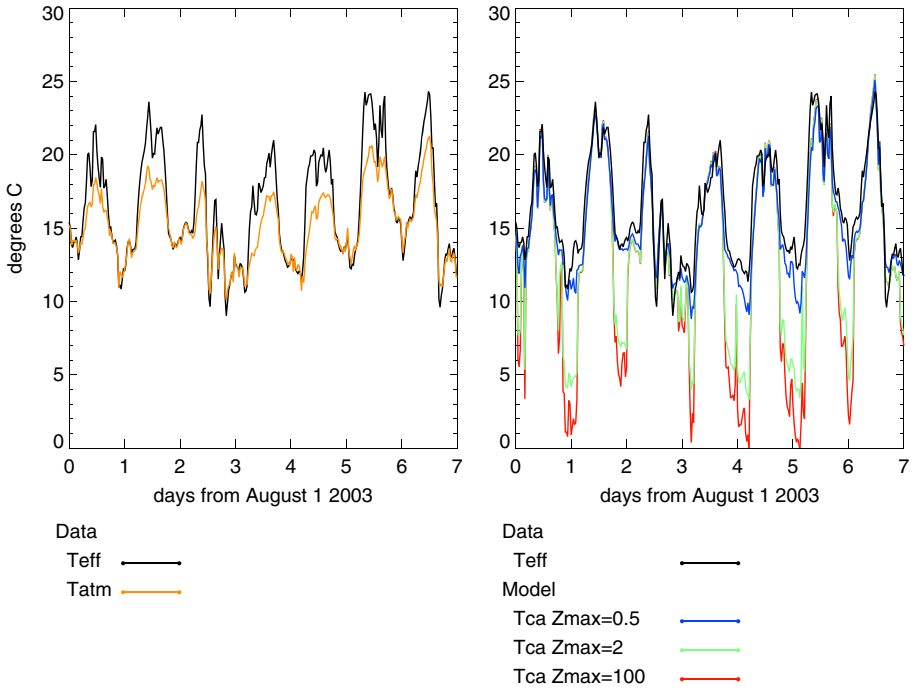

Figure 2. Temperature in degrees Celsius. (left panel) Measured atmospheric air temperature at 21.5 m (T_{atm}, orange line) and effective canopy temperature (T_{eff}, black line). (right panel) T_{eff} and CLM canopy air temperature (T_{ca}) for three values of ζ_{max} (blue = 0.5; green = 2; red = 100).

ζ_{max} = 100, T_{ca} must decrease well below T_{atm} in order to develop a temperature gradient large enough to overcome the aerodynamic resistance. By constraining ζ, the resistance is capped and higher sensible heat fluxes are obtained in stable conditions. Note, however, that because of this cap, these resistances are no longer consistent with the temperature states under Monin-Obukhov stability theory.

4.3. Surface Energy Fluxes

The effect of the stability cap on the fluxes of sensible heat and momentum is shown in Figure 3, which compares CLM simulations having ζ_{max} = 0.5 and ζ_{max} = 100. Diel cycles are calculated by averaging from June through August for the period 2003 to 2013. The daytime portion of the diel cycles of H, u_*, and R_h are similar for both simulations, but during the night they behave differently. The sensible heat flux in the ζ_{max} = 0.5 simulation is more negative than observed, which is due to higher u_* and low R_h during the night. In contrast, the ζ_{max} = 100 simulation has less negative H, corresponding to lower u_* and much higher R_h during the night. Figure 3 also shows that during the day, both simulations overpredict sensible heat by about 50 W/m^2.

Figure 4 compares the observed surface energy diel cycle to that simulated by CLM. The observed partitioning of net radiation R_{net} mainly into sensible H and latent L heat fluxes with a relatively small ground heat flux G is broadly reproduced by both CLM simulations. A key difference is that the observed energy fluxes do not sum to zero and a significant residual equal to $R_{net} - H - L - G$ exists. In CLM, by construction, the sum of these terms is identically zero. Leuning et al. (2012) concluded that while measurement errors may contribute to the nonzero residual of measured surface energy fluxes, they are unlikely to be the primary source of the differences, which can be as large as 100 W/m^2 at the half-hourly time scale. Instead, a substantial part of the imbalance can be explained by heat stored in soils, air, and biomass within the canopy (Leuning et al., 2012). Burns et al. (2015) and Turnipseed et al. (2002) showed that some of the residual of the observed Niwot Ridge surface energy fluxes is due to heat stored in vegetation biomass. These studies found that the largest component of heat storage was in the tree boles (i.e., tree trunks) followed by storage by the tree needles; heat stored in the canopy air was considerably smaller. Because CLM lacks these heat storage components, sensible, latent, and ground heat fluxes alone must match net radiation, leading to the overestimation of sensible heat flux shown in Figure 3. In section 5, we describe modifications to the CLM canopy energy budget to account for heat stored in vegetation biomass and examine the effect of this heat storage on simulated energy fluxes, temperature states, and atmospheric stability.

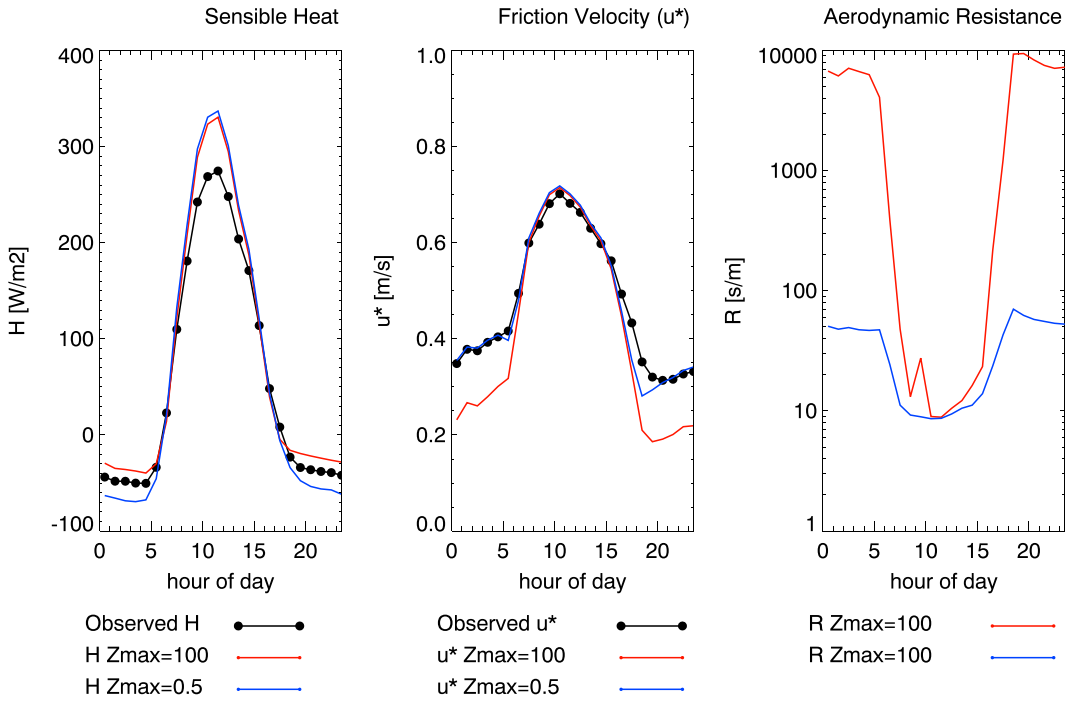

Figure 3. Mean diel (24-hr) cycle of sensible heat (left panel), u_* (middle panel), and aerodynamic resistance to sensible heat (left panel). Black lines show observations, blue line shows Community Land Model simulation having ζ_{max} = 0.5, red line shows Community Land Model simulation having ζ_{max} = 100.

5. Biomass Heat Storage

To incorporate forest BHS in CLM, we conceptualize the big leaf canopy as consisting of leaves, which are photosynthetically active and transpire, and stems, which account for nontranspiring structural material such as trunks and branches. The transmission, reflection, and absorption of radiation by the canopy is unchanged, but heat may now be stored within the canopy. The BHS of the leaf and stem vegetation components is represented by new temperature state variables T_{leaf} and T_{stem}, respectively. The air within the canopy is assumed to have negligible capacity to store heat so that the sensible heat flux H between the canopy air space and the atmosphere must be balanced by the sum of the sensible heat from the leaves H_{leaf}, stems H_{stem}, and the ground H_g

$$H_{atm} = H_{leaf} + H_{stem} + H_g. \tag{3}$$

The canopy air space temperature now depends on the separate leaf and stem temperatures according to

$$T_{ca} = \frac{c^h_{atm}T_{atm} + c^h_g T_g + c^h_{leaf}T_{leaf} + c^h_{stem}T_{stem}}{c^h_{atm} + c^h_g + c^h_{leaf} + c^h_{stem}}. \tag{4}$$

5.1. Stem Energy Balance

Change in the temperature of the stem portion of the canopy is determined by

$$\vec{S}_{stem} + \vec{L}_{stem}\left(T_{stem}\right) - H_{stem}\left(T_{stem}\right) = C_{stem}\frac{dT_{stem}}{dt}, \tag{5}$$

where $\vec{S}_{stem}$ is the solar radiation absorbed by the stems, $\vec{L}_{stem}$ is the net longwave radiation absorbed by the stems, H_{stem} is the sensible flux from the stems to the canopy air space, and C_{stem} is the heat capacity of the stems.

The radiation absorbed by stems is assumed to be a fraction of the radiation absorbed by the canopy

$$\vec{S}_{stem} = f_{stem}\vec{S}_{canopy}, \tag{6}$$

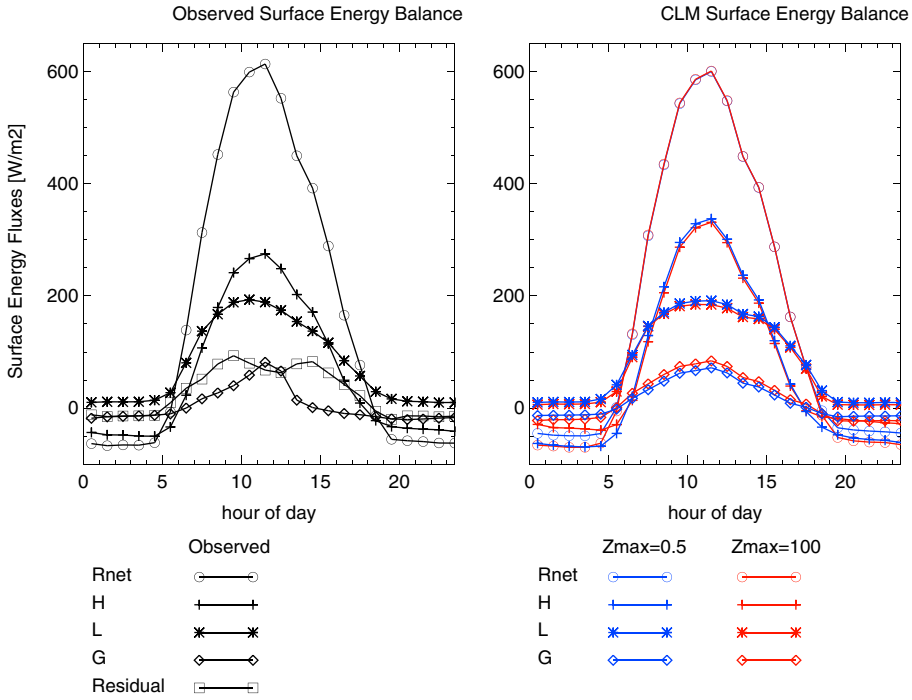

Figure 4. Mean diel cycle of surface energy fluxes of net radiation R_{net}, sensible heat H, latent heat L, ground heat G (W/m^2). (left panel) Observed; dashed line shows residual $R_{net} - H - L - G$. (right panel) CLM; residual is zero. CLM = Community Land Model.

$$\vec{L}_{stem} = f_{stem}\,\vec{L}_{canopy}, \tag{7}$$

where L and S are the leaf and stem area indices (m^2/m^2), respectively, and the stem fraction is

$$f_{stem} = k_{vert}\frac{SAI}{LAI + SAI}, \tag{8}$$

where LAI is the LAI (m^2/m^2), SAI is the stem area index (m^2/m^2), and k_{vert} is a parameter to account for the vertical distribution through the canopy of stem area. A value of k_{vert} near 1 would imply a greater portion of the stems near the upper canopy, while a value near 0 would imply more of the stem area near the ground.

The areametric heat capacity of the stems, C_{stem} [J·m^{-2}·K^{-1}], is the sum of the heat capacities of the dry wood and of the water contained in the stems multiplied by the mass of biomass per area

$$C_{stem} = \left(c_{dry} + \frac{f_w}{1 - f_w}c_{water}\right) M_{tree}, \tag{9}$$

where c_{dry} = 1,400 J·kg^{-1}·K^{-1} is the heat capacity of the dry wood, c_{water} = 4,188 J·kg^{-1}·K^{-1} is the heat capacity of water, and f_w = 0.45 is the assumed fraction of fresh biomass that is water (Bonan et al., 2018). The tree dry mass per area is calculated as

$$M_{tree} = N_{tree}\,\rho_{wood}\,V_{tree}, \tag{10}$$

where ρ_{wood} = 500 kg/m^3 is the density of dry wood, N_{tree} = 0.4 m^{-2} is the number of trees per square meter (Burns et al., 2018), and V_{tree}, the individual tree volume, is calculated by assuming that trees are cylindrical

$$V_{tree} = k_V\,\pi\left(\frac{D_{bh}}{2}\right)^2 h_{tree}, \tag{11}$$

where D_{bh} = 0.2 m is the mean breast-height diameter and h_{tree} = 13 m is the mean tree height at the Niwot Ridge site. k_V is an adjustable parameter to account for the departure of tree volume from a cylinder.

The sensible heat flux from the stems to the canopy air space is

$$H_{stem} = -\rho_{atm} C_p \frac{\left(T_{ca} - T_{stem}\right)}{r_{stem}}, \tag{12}$$

where ρ_{atm} (kg/m^3) is the density of air, C_p is the heat capacity of air (J·kg^{-1}·K^{-1}). The stem resistance to sensible heat is

$$r_{stem} = \frac{\left(r_b + r_{bole}\right)}{A_{stem}}, \tag{13}$$

where r_b is the vegetation boundary layer resistance (s/m; Oleson et al., 2013) and r_{bole} is the resistance to heat transfer between the interior of the tree and the tree surface (s/m). A_{stem} is the surface area of the stems per unit ground area

$$A_{stem} = N_{tree}\, k_A \left(\pi D_{bh}\right) h_{tree}, \tag{14}$$

where k_A is an adjustable parameter to account for the departure of tree area from a cylinder. In this study, k_V and k_A were both set equal to 1.

5.2. Leaf Energy Balance

Change in the temperature of the leaves within the canopy is given by

$$\vec{S}_{leaf} + \vec{L}_{leaf}\left(T_{leaf}\right) - H_{leaf}\left(T_{leaf}\right) - \lambda E_{leaf}\left(T_{leaf}\right) = C_{leaf}\frac{dT_{leaf}}{dt}, \tag{15}$$

where $\vec{S}_{leaf}$ is the solar radiation absorbed by the leaves, $\vec{L}_{leaf}$ is the net longwave radiation absorbed by the leaves, H_{leaf} and λE_{leaf} are the sensible and latent heat fluxes from the leaves, respectively, and C_{leaf} is the heat capacity of the leaves. λ is the latent heat of vaporization (J/kg).

The radiation absorbed by leaves is assumed to be a constant fraction of the radiation absorbed by the canopy

$$\vec{S}_{leaf} = f_{leaf}\,\vec{S}_{canopy} \tag{16}$$

$$\vec{L}_{leaf} = f_{leaf}\,\vec{L}_{canopy}, \tag{17}$$

where the leaf fraction is

$$f_{leaf} = 1 - f_{stem}. \tag{18}$$

The sensible heat flux from the leaves to the canopy air space is given by

$$H_{leaf} = -\rho_{atm} C_p \cdot \frac{\left(T_{ca} - T_{leaf}\right)}{r_{leaf}}, \tag{19}$$

where

$$r_{leaf} = \frac{r_b}{A_{leaf}} \tag{20}$$

and A_{leaf} is surface area of the leaves per unit ground area

$$A_{leaf} = 2\,LAI, \tag{21}$$

where LAI is the LAI (m^2/m^2).

The areametric heat capacity of the leaves C_{leaf} (J·m^{-2}·K^{-1}) is the sum of the heat capacities of the dry leaves and of the water contained in the leaves multiplied by the dry leaf mass per area

$$C_{leaf} = \left(c_{dry} + \frac{f_w}{1 - f_w} c_{water}\right) M_{leaf}, \tag{22}$$

where

$$M_{leaf} = M_a\, LAI \tag{23}$$

and M_a = 0.25 kg/m^2 is the leaf mass per leaf area (Bonan et al., 2018).

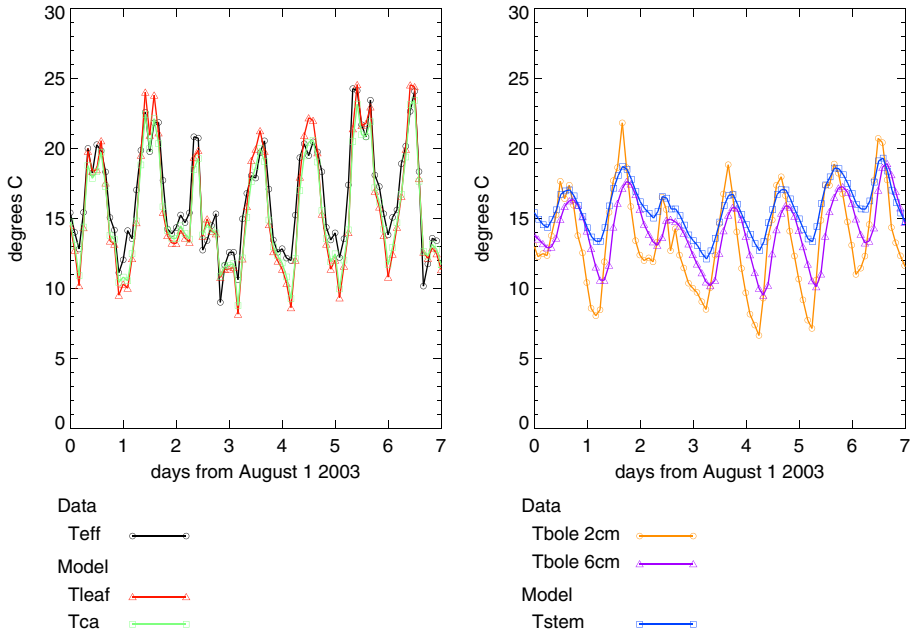

Figure 5. Temperature in degrees Celsius. (left panel) Effective canopy temperature (T_{eff}, black line), CLM canopy air temperature (T_{ca}, green line), CLM leaf temperature (T_{leaf}, red line). (right panel) Observed bole temperatures at 1.5-m height and depths of 2m (orange line) and 6 cm (purple line), CLM stem temperature (T_{stem}, blue line). CLM = Community Land Model.

6. Results

6.1. Canopy Temperature

With the modifications described in section 5, we performed a CLM simulation (BHS) and assessed its performance against the Niwot Ridge AmeriFlux site observations. The values of parameters used in the BHS simulation are shown in Table 1. It is important to note that in this simulation the constraint on atmospheric stability was removed, that is, $\zeta_{max} = 100$. Figure 5 (left panel) shows that the simulated canopy temperature in the BHS simulation closely tracks the observed radiative canopy temperature, particularly during the day. At night, T_{ca} is typically lower than T_{eff} by 1–2 °C, and at times as much as 5 °C. This can be compared to the $\zeta_{max} = 100$ simulation shown in Figure 2, in which T_{ca} was typically 5–15 °C cooler than T_{eff}. Figure 5 also shows that the leaf temperature is slightly higher during the day and slightly lower at night than the canopy air temperature. The right panel of Figure 5 compares bole temperatures measured at 2 and 6 cm depth (Burns et al., 2015). The variation of the shallower measurements more closely resembles the canopy air temperatures in magnitude and phase, while the deeper bole temperature measurements are damped and reach daily minimum values later. The BHS stem temperature varies with an amplitude about half that of the canopy temperature and is shifted later by about 3 hr, which is more similar to the 6-cm bole temperatures.

To show the impact of BHS over a longer time period, Figure 6 shows half-hourly canopy temperatures from observations T_{eff} and CLM T_{ca} for the period June through September 2003. In the left column, one can see that T_{ca} in the $\zeta_{max} = 100$ simulation is typically overestimated during the day, and greatly underestimated at night when it often drops below freezing. In contrast, the BHS canopy temperatures only rarely depart substantially from the observed canopy temperature.

Figure 7 (left panel) shows the mean diel cycle of canopy temperature, averaged from June through August for the period 2003 to 2013. Midday canopy temperatures from both CLM simulations agree closely with T_{eff}, while T_{ca} from the BHS simulation is about 5 °C higher at night than the $\zeta_{max} = 100$ simulation. The temperature of the vegetation components are shown in the right panel of Figure 7. Both the $\zeta_{max} = 100$ bulk leaf temperature and the BHS leaf temperature peak around noon, and the BHS leaf temperature is about a degree cooler at midday. At night, the BHS leaf temperature is slightly cooler than the canopy temperature, while the $\zeta_{max} = 100$ bulk leaf temperature is about 5 °C cooler. The BHS stem temperature peaks later in the day, and is cooler during the day, but warmer at night than both the canopy and leaf temperatures. The amplitude

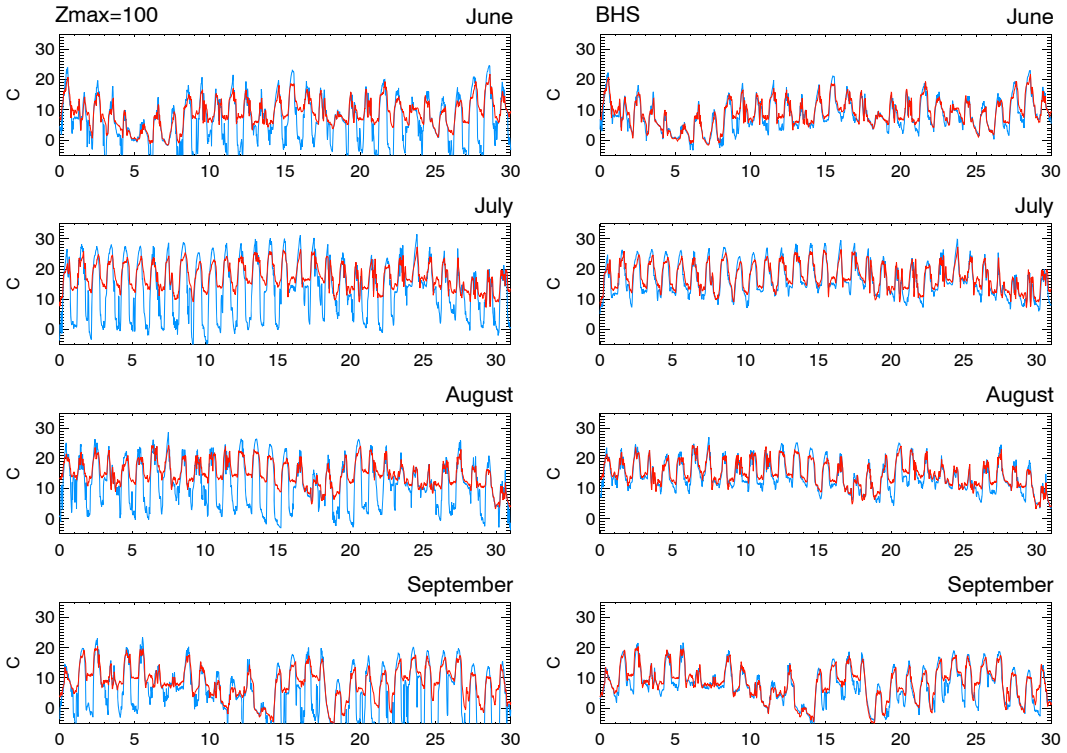

Figure 6. Canopy temperature for the months June through September 2003. (left column) ζ_{max} = 100 simulation; (right column) BHS simulation. Red lines are observed effective canopy temperature, blue lines are Community Land Model simulated canopy air temperature. BHS = biomass heat storage.

of the BHS stem temperature is similar to the observed 6-cm bole temperature, while the phase is earlier by around 2 hr.

6.2. Atmospheric Stability and Aerodynamic Resistance

Although the constraint on ζ_{max} was removed for the BHS simulation, the nighttime friction velocity does not become biased low, as is the case in the ζ_{max} = 100 simulation (Figure 8, left panel). Instead, the mean diel cycle of friction velocity agrees well with the observed (Figure 8, middle panel). The heat released from the tree stems at night maintains a warmer canopy air space, and therefore less stable conditions and higher friction velocities. The larger nighttime friction velocities result in sensible heat resistances that are about 10 times lower (Figure 8, right panel), such that the canopy energy balance can be maintained by a smaller temperature gradient between the atmosphere and canopy while yielding a similar magnitude of sensible heat flux in the two simulations. Figure 8 also shows that the effect of the BHS reduces the high bias in daytime sensible heat flux seen in both of the simulations in Figure 3. Instead of immediately raising the temperature of the vegetation and therefore increasing the sensible heat flux, some of the net radiation is stored in the stems, whose temperature increases more slowly due to its higher heat capacity. The BHS increases during the day and decreases at night, consistent with observational estimates of the change in tree bole heat storage made by Burns et al. (2015).

6.3. Additional Flux Measurement Sites

To test whether the BHS modifications would impart a consistent change to the simulated surface energy balance for a variety of climate conditions and vegetation characteristics, additional simulations were performed for 11 sites spanning the 8 tree PFTs defined in CLM. The locations of the sites are plotted in Figure 9, and the geographical coordinates, PFT, and observation period are shown in Table 2. All simulations used local meteorological forcing data observed at the flux measurement sites.

Figure 10 (left panel) shows that the sum of the observed midday (10–14 hr) mean sensible and latent heat fluxes are typically less than observed net radiation by 50–100 W/m^2 across all sites; similar behavior is shown by the BHS simulations. In contrast, the ζ_{max} = 100 simulations are close to the 1:1 line for almost all locations. The right panel of Figure 10 shows that the modeled latent heat fluxes are similar in the two simulations, and

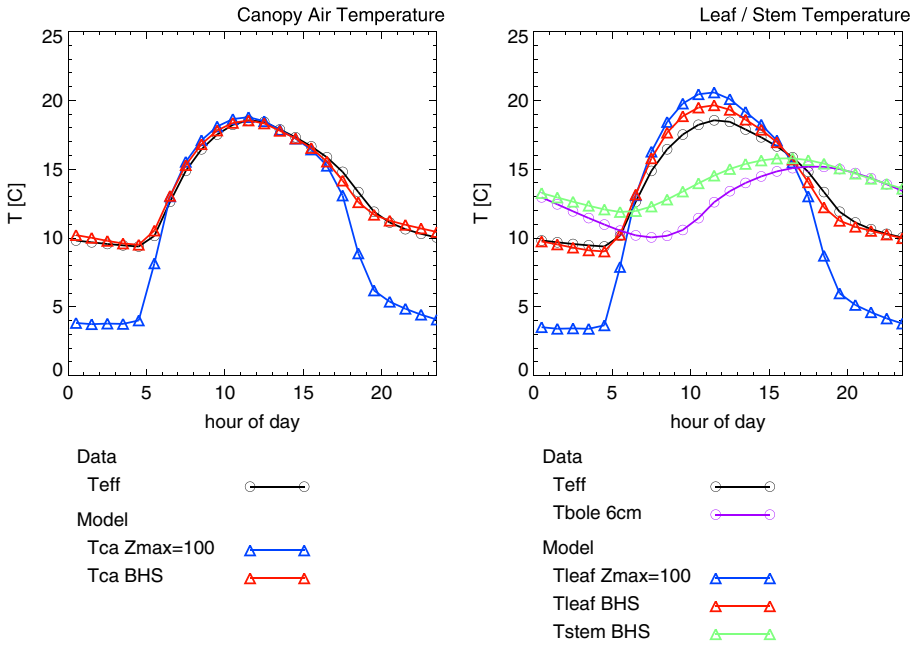

Figure 7. (left panel) Diel cycle of canopy temperature. T_{eff} (black line), ζ_{max} = 100 T_{ca} (blue line), BHS T_{ca} (red line). (right panel) Diel cycle of canopy and vegetation temperatures. T_{eff} (black line), $T_{bole,6cm}$ (magenta line), ζ_{max} = 100 T_{leaf} (blue line), BHS T_{leaf} (red line), BHS T_{stem} (green line). BHS = biomass heat storage.

furthermore that they agree well with the observations. The modeled sensible heat fluxes in the BHS simulation agree well with the observations, but are higher than observed in the ζ_{max} = 100 simulation. Figure 10 thus indicates that in the absence of BHS, sensible heat flux is overpredicted for all sites, and this high bias is the main cause of the inability of the ζ_{max} = 100 simulation to match the observed relationship between net radiation and the sum of the sensible and latent heat fluxes.

The ratio of $L+H$ to R_{net} is around 0.9 for most sites in the ζ_{max} = 100 simulation (Figure 11, left panel). Including the effect of BHS reduces this ratio by 0.1–0.2, bringing the simulated ratios into closer agreement with the observed values. The biases in midday latent heat fluxes are increased at some sites by about 10–20 W/m^2, while the biases in sensible heat fluxes are decreased by 40–80 W/m^2 (Figure 11, right panel).

6.4. Global Simulations

Figures 10 and 11 show that the effect of BHS has a robust positive impact on the simulations for all of the flux measurement sites. To examine the impact on the model at other locations, we performed three global simulations: an unconstrained stability simulation (ζ_{max} = 100), a constrained stability simulation (ζ_{max} = 0.5; the CLM5 default value), and a BHS simulation. These model runs used atmospheric boundary conditions for the period 2001–2010 from the Global Soil Wetness Project (Kim, 2017). The spatial resolution of the simulations is 1.25° longitude × 0.9° latitude. For the BHS simulation, we used the parameter values listed in Table 1, except for the following: D_{bh} = 0.3 m, N_{tree} = 0.2 m^{-2}, and h_{tree}, whose value was assigned based on the standard CLM pft-specific values (Oleson et al., 2013).

Figure 12 shows the ζ_{max} = 100 annual mean daily canopy air temperature, the annual mean daily minimum and maximum temperatures (top row), and the differences in temperatures between the ζ_{max} = 100 and the ζ_{max} = 0.5 (middle row) and BHS simulations (bottom row). Relative to the ζ_{max} = 100 simulation, the ζ_{max} = 0.5 canopy air temperature map shows the largest differences in the boreal forests, with temperatures 1–2 °C warmer. Tropical and temperate forests show smaller temperature differences, with less than 0.5 °C warming apparent in these areas. A comparison of the mean annual daily minimum and maximum temperatures indicates that the warmer mean daily canopy temperatures are primarily due to a large increase in the daily minimum temperature, while the daily maximum temperature shows only a modest increase. In the BHS simulation, the mean annual daily canopy air space temperature shows only minor differences with respect to the ζ_{max} = 100 simulation. Like the constrained (ζ_{max} = 0.5) simulation, the daily minimum temperature shows

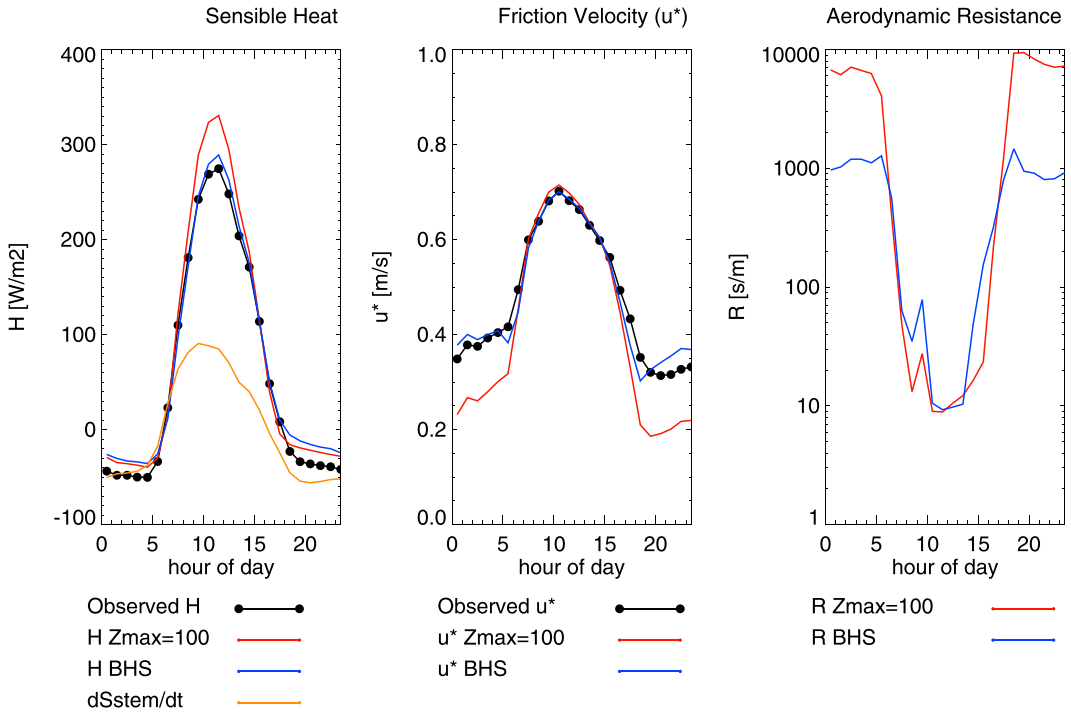

Figure 8. Mean diel (24-hr) cycle of sensible heat (left panel), u_* (middle panel), and aerodynamic resistance to sensible heat (left panel). Black lines show observations, blue line shows Community Land Model BHS simulation, red line shows Community Land Model simulation having ζ_{max} = 100. The change in heat stored by the biomass is shown by the orange line in the left panel. BHS = biomass heat storage.

a large increase; in contrast, however, the daily maximum temperature differences are negative, that is, the peak daytime temperatures are reduced in the BHS simulation. The net result is that mean annual canopy air temperatures in the BHS simulation are not significantly different from those in the ζ_{max} = 100 simulation, despite the difference in the temperature range at the subdaily timescale.

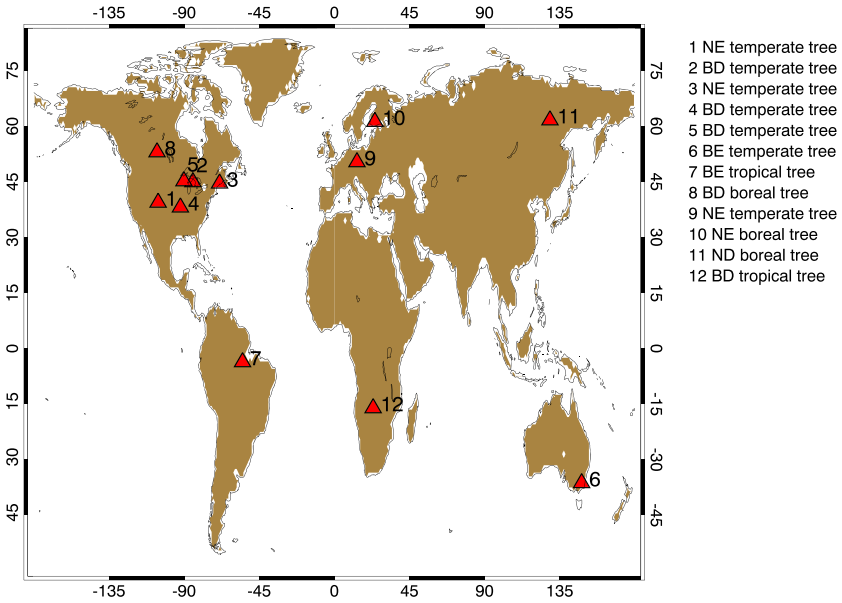

Figure 9. Map of flux measurement sites.

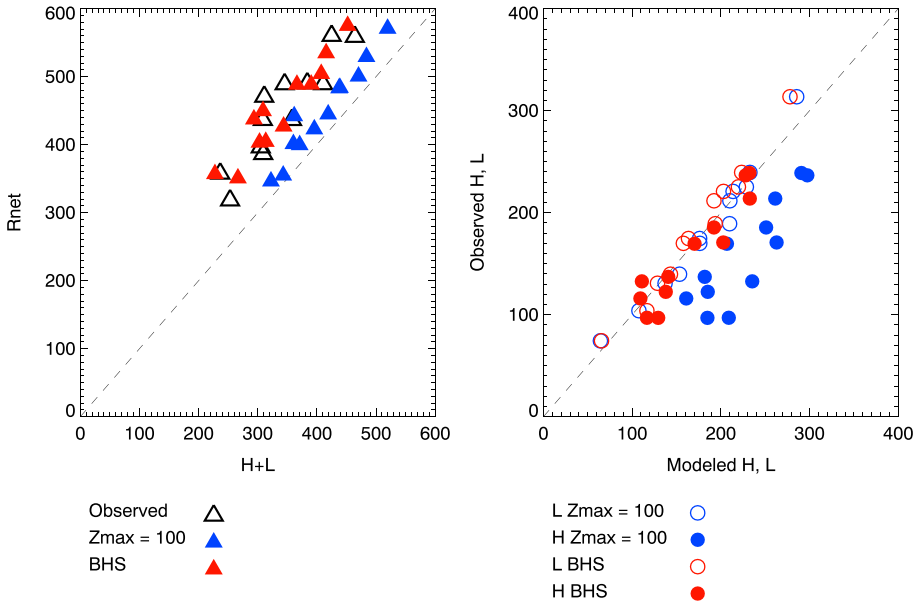

Figure 10. (left panel) Sum of sensible and latent heat fluxes (*x* axis) plotted against net radiation flux (*y* axis). Black triangles are observed, blue triangles are Community Land Model ζ_{max} = 100, and red triangles are Community Land Model BHS. Each triangle represents the mean midday flux (W/m^2). (right panel) Modeled versus observed sensible (closed circles) and latent (open circles) heat fluxes. BHS = biomass heat storage.

Figure 12 also shows that in nonforested regions, for example, grasslands, the presence of BHS has little effect on either mean annual canopy air temperature or minimum/maximum temperatures. Reducing the stability cap to 0.5 has a modest warming effect in some nonforested locations, such as parts of Africa and Europe.

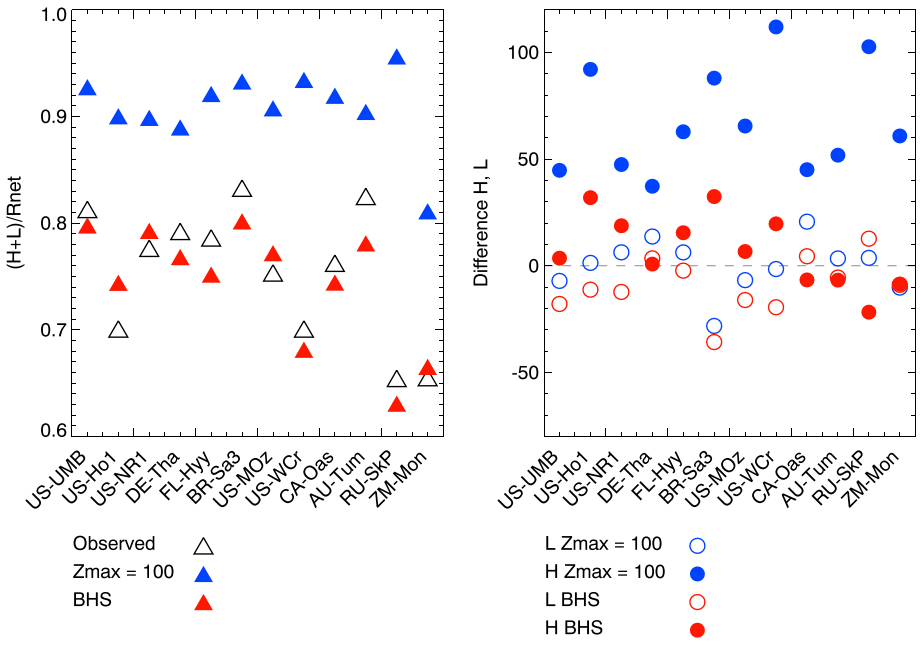

Figure 11. (top panel) Ratio of the sum of sensible and latent heat fluxes to net radiation. Black circles are observed, blue circles are Community Land Model ζ_{max} = 100, and red circles are Community Land Model BHS. (bottom panel) Modeled minus observed sensible (closed circles) and latent (open circles) heat fluxes (W/m^2). BHS = biomass heat storage.

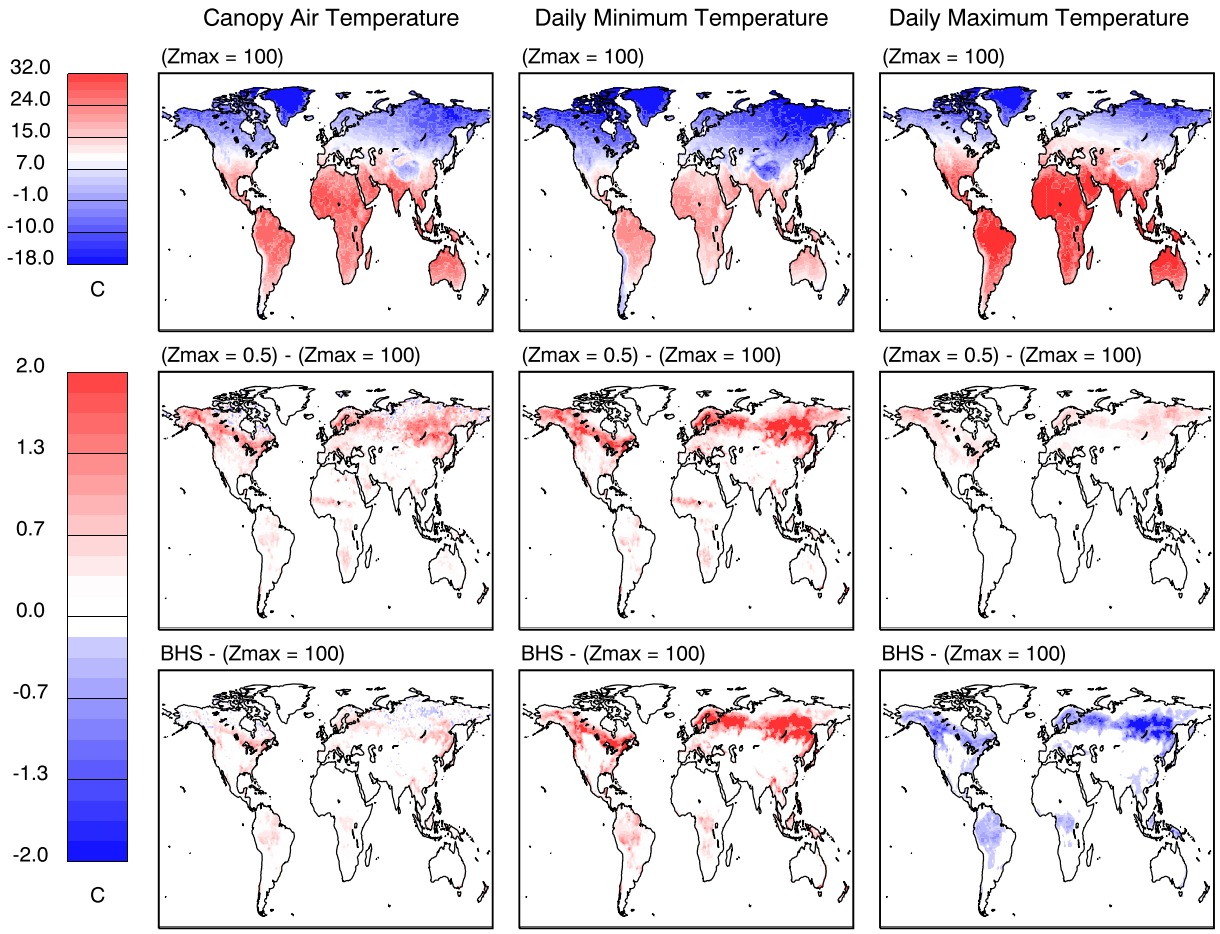

Figure 12. (top row) Mean annual canopy air space temperature (left), mean annual daily minimum temperature (center), mean annual daily maximum temperature (right) for ζ_{max} = 100 simulation. (middle row) Temperature differences between ζ_{max} = 0.5 and ζ_{max} = 100 simulations. (bottom row) Temperature differences between BHS and ζ_{max} = 100 simulations. BHS = biomass heat storage.

7. Discussion

In this study, the inclusion of heat stored in biomass has been shown to simultaneously reduce multiple biases with respect to observations: low nighttime canopy temperatures, low nighttime friction velocity, and high midday sensible heat flux. CLM implements a cap on the Monin-Obukhov stability parameter that constrains nighttime surface temperatures from becoming too low. This method of preventing the decoupling of the land surface from the atmosphere during stable atmospheric conditions has also been applied in the NCEP Global Forecast System by Zheng et al. (2017), who showed significant reductions in 2-m temperature biases with this approach. Capping the Monin-Obukhov stability parameter is an alternative means of constraining nighttime temperature and friction velocity, but generally does not affect temperature or sensible heat flux during the day, when atmospheric conditions are typically neutral or unstable. Furthermore, a fixed upper limit on ζ is not typically observed (Businger et al., 1971; Pahlow et al., 2001; Zhang et al., 2010). Because the heat capacity of the vegetation reduces the rate at which the temperature decreases at night, conditions in the BHS simulation remain closer to neutral and an arbitrary limit on the model's stability parameter becomes unnecessary.

A key feature of this implementation is the inclusion of separate heat reservoirs for leaves and stems. Because of their larger ratio of surface area to heat capacity, leaves respond rapidly to environmental conditions, while stems respond more slowly, buffering the canopy airspace temperature. We hypothesize that models that ignore biomass heat capacity (e.g., previous versions of CLM; Noah-MP; Niu et al., 2011) consider a lumped vegetation/soil layer (e.g., ORCHIDEE; Krinner et al., 2005) or use a single bulk vegetation heat capacity

Acknowledgments
We thank Gordon Bonan and Ronny Meier for helpful discussions that greatly benefited this work. We also thank D. Clark and an anonymous reviewer for their valuable suggestions that improved this paper. The National Center for Atmospheric Research is sponsored by the National Science Foundation. Computing resources (doi:10.5065/D6RX99HX) were provided by the Climate Simulation Laboratory at NCAR's Computational and Information Systems Laboratory, sponsored by the National Science Foundation and other agencies. D.L. was supported in part by the RUBISCO Scientific Focus Area (SFA), which is sponsored by the Regional and Global Climate Modeling (RGCM) Program in the Climate and Environmental Sciences Division (CESD) of the Office of Biological and Environmental Research in the U.S. Department of Energy Office of Science. The US-NR1 AmeriFlux site and contributions by S.B. have been supported by the U.S. DOE, Office of Science through the AmeriFlux Management Project (AMP) at Lawrence Berkeley National Laboratory under award 7094866. S.B. has also been partially supported by NIFA/USDA grant 201567003-23485. We acknowledge the following AmeriFlux sites for their data records: US-NR1, US-UMB, US-Ho1, US-MOz, US-WCr. In addition, funding for AmeriFlux data resources was provided by the U.S. Department of Energys Office of Science. AmeriFlux data were obtained from http://ameriflux.lbl.gov/ for the following sites: US-Ho1, https://doi.org/10.17190/AMF/1246061; US-NR1, https://doi.org/10.17190/AMF/1246088; US-UMB, https://doi.org/10.17190/AMF/1246107; US-MOz, https://doi.org/10.17190/AMF/1246081; US-WCr, https://doi.org/10.17190/AMF/1246111. This work used eddy covariance data acquired and shared by the FLUXNET community, including these networks: AmeriFlux, AfriFlux, AsiaFlux, CarboAfrica, CarboEuropeIP, CarboItaly, CarboMont, ChinaFlux, Fluxnet-Canada, GreenGrass, ICOS, KoFlux, LBA, NECC, OzFlux-TERN, TCOS-Siberia, and USCCC. We acknowledge the following FLUXNET2015 Data set sites for their data records: AU-Tum, BR-Sa3, CA-Oas, DE-Tha, FL-Hyy, RU-SkP, ZM-Mon. FLUXNET2015 data were obtained from http://fluxnet.fluxdata.org/ for the following sites: AU-Tum, DOI: 10.18140/FLX/1440126; BR-Sa3, DOI: 10.18140/FLX/1440033; CA-Oas, DOI: 10.18140/FLX/1440043; DE-Tha, DOI: 10.18140/FLX/1440152; FL-Hyy, DOI: 10.18140/FLX/1440158; RU-SkP, DOI: 10.18140/FLX/1440243; ZM-Mon, DOI: 10.18140/FLX/1440189. CLM Code can be found at https://github.com/swensosc/ctsm/tree/heat_storage_biomass.

(e.g., JULES; Best et al., 2011) will be unable to capture both the fast and slow thermodynamic response of the vegetation canopy in locations having significant biomass.

All of the sites in this study showed a significant reduction in bias for midday sensible heat fluxes, but latent heat flux biases were slightly degraded for seven of the sites. Because the mean daily biases are quite similar for the two simulations (not shown), the higher midday biases indicate that the timing of latent heat flux has shifted slightly later in the day in response to the changes in leaf and canopy air temperature. Biases in latent heat may be related to afternoon suppression of stomatal conductance due to plant water depletion (Matheny et al., 2014), which CLM cannot simulate because it does not explicitly represent plant water storage.

As discussed by Leuning et al. (2012), there are multiple possible sources of the energy imbalance problem. Heat stored in vegetation biomass is not the only term that may be missing from the CLM surface energy balance, nor the only reason why the simulated surface energy budget may not agree with the observed surface energy budget. CLM does not presently account for changes in sensible and latent heat in the canopy airspace, nor the energy absorbed in photosynthesis or heat released by respiration, which can make non-negligible contributions to the surface energy budget (Meyers & Hollinger, 2004). In addition, measurement errors and the effects of lateral advection and nonhomogeneous landscapes may be present in the observational data (Stoy et al., 2013). Despite these potential issues, the results presented here indicate that significant improvements in surface energy balance closure in forested regions can be obtained by including biomass heat storage. Because the diel cycle of the surface energy balance influences the evolution of the boundary layer and cloud formation (Betts, 2009), future work will assess the impact of BHS on land-atmosphere interactions in the coupled model system. Additional subsequent research addressing other unmodeled surface energy budget terms, for example, sensible heat storage in the canopy air space, may further reduce some biases.

The parameterization developed here introduces several new parameters into CLM that characterize the shape and distribution of biomass within the canopy. Some are more readily available than others. For example, D_{bh} and N_{tree} can be obtained from field site surveys or forestry inventories. In contrast, k_{vert}, k_V, and k_A are not available, but in principle could be estimated from forest lidar imagery. Ongoing and future research will examine the sensitivity of the surface energy balance to variations in these parameters, especially in the context of within-pft variability due to differences between species and age classes.

8. Summary

CLM4.5 simulations of Niwot Ridge surface climate exhibit biases in nighttime canopy air temperature and friction velocity that were shown to relate to atmospheric stability corrections (Burns et al., 2018). To reduce these biases, a more stringent stability cap ($\zeta_{max} = 0.5$) was implemented in CLM5 (Oleson et al., 2013). In this study, we have shown that an alternative method of reducing the nighttime temperature bias is to include the storage of heat within vegetation biomass and the exchange of that heat with the canopy air space. For locations having large amounts of biomass (i.e., forests), this approach results in further improvements to daytime sensible heat and canopy air temperature, which are typically not affected by changing the maximum stability parameter for stable conditions. For nonforested locations having low biomass amounts, the BHS parameterization provides similar results to a simulation lacking a representation of vegetation heat storage.

References

Best, M. J., Abramowitz, G., Johnson, H. R., Pitman, A. J., Balsamo, G., Boone, A., et al. (2015). The plumbing of land surface models: Benchmarking model performance. *Journal of Hydrometeorology*, *16*, 1425–1442. https://doi.org/10.1175/JHM-D-14-0158.1

Best, M. J., Pryor, M., Clark, D. B., Rooney, G. G., Essery, R. L. H., Menard, C. B., et al. (2011). The Joint UK Land Environment Simulator (jules), model description. Part 1: Energy and water fluxes. *Geoscientific Model Development*, *4(3)*, 677–699. https://doi.org/10.5194/gmd-4-677-2011

Betts, A. K. (2009). Land-surface-atmosphere coupling in observations and models. *Journal of Advances in Modeling Earth Systems*, *1*, 4. https://doi.org/10.3894/JAMES.2009.1.4

Blanken, P. D., Monson, R. K., Burns, S. P., & Turnipseed, A. A. (1998–present). *Data and information for the AmeriFlux US-NR1 Niwot Ridge subalpine forest (LTER NWT1) site, AmeriFlux management project*. Berkeley, CA: Lawrence Berkeley National Laboratory. https://doi.org/10.17190/AMF/1246088

Bonan, G. B. (2015). *Ecological climatology: Concepts and applications*. Cambridge: Cambridge University Press.

Bonan, G. B., Patton, E. G., Harman, I. N., Oleson, K. W., Finnigan, J. J., Lu, Y., & Burakowski, E. A. (2018). Modeling canopy-induced turbulence in the Earth system: A unified parameterization of turbulent exchange within plant canopies and the roughness sublayer (CLM-ml v0). *Geoscientific Model Development*, *11*, 1467–1496. https://doi.org/10.5194/gmd-11-1467-2018

Burns, S. P., Blanken, P. D., Turnipseed, A. A., Hu, J., & Monson, R. K. (2015). The influence of warm-season precipitation on the diel cycle of the surface energy balance and carbon dioxide at a Colorado subalpine forest site. *Biogeosciences*, *12*, 7349–7377. https://doi.org/10.5194/bg-12-7349-2015

Burns, S. P., Swenson, S. C., Wieder, W. R., Lawrence, D. M., Bonan, G. B., Knowles, J. F., & Blanken, P. D. (2018). A comparison of the diel cycle of modeled and measured latent heat flux during the warm season in a Colorado subalpine forest. *Journal of Advances in Modeling Earth Systems*, *10*, 617–651. https://doi.org/10.1002/2017MS001248

Businger, J. A., Wyngaard, J. C., Izumi, Y., & Bradley, E. F. (1971). Flux-profile relationships in the atmospheric surface layer. *Journal of Atmospheric Sciences*, *28*(2), 181–189. https://doi.org/10.1175/1520-0469(1971)

Haughton, N., Abramowitz, G., Pitman, A. J., Or, D., Best, M. J., Johnson, H. R., et al. (2016). The plumbing of land surface models: Is poor performance a result of methodology or data quality? *Journal of Hydrometeorology*, *17*, 1705–1723. https://doi.org/10.1175/JHM-D-15-0171.1

Haverd, V., Cuntz, M., Leuning, R., & Keith, H. (2007). Air and biomass heat storage fluxes in a forest canopy: Calculation within a soil vegetation atmosphere transfer model. *Agricultural and Forest Meteorology*, *147*, 125–139. https://doi.org/10.1016/j.agrformet.2007.07.006

Hurrell, J. W., Holland, M. M., Gent, P. R., Ghan, S., Kay, J. E., Kushner, P. J., et al. (2013). The community earth system model: A framework for collaborative research. *Bulletin of the American Meteorological Society*, *94*(9), 1339–1360. https://doi.org/10.1175/bams-d-12-00121.1

Kim, H. (2017). Global soil wetness project phase 3 atmospheric boundary conditions (experiment 1). Data Integration and Analysis System (DIAS) https://doi.org/10.20783/DIAS.501

Krinner, G., Viovy, N., de Noblet-Ducoudr, N., Oge, J., Polcher, J., Friedlingstein, P., et al. (2005). A dynamic vegetation model for studies of the coupled atmosphere-biosphere system. *Global Biogeochemical Cycles*, *19*, GB1015. https://doi.org/10.1029/2003GB002199

Lawrence, D. M., Oleson, K. W., Flanner, M. G., Thornton, P. E., Swenson, S. C., Lawrence, P. J., et al. (2011). Parameterization improvements and functional and structural advances in version 4 of the community land model. *Journal of Advances in Modeling Earth Systems*, *3*, M03001. https://doi.org/10.1029/2011MS000045

Leuning, R., van Gorsela, E., Massman, W. J., & Isaac, P. R. (2012). Reflections on the surface energy imbalance problem. *Agricultural and Forest Meteorology*, *156*, 65–74. https://doi.org/10.1016/j.agrformet.2011.12.002

Lindroth, A., Molder, M., & Lagergren, F. (2010). Heat storage in forest biomass improves energy balance closure. *Biogeosciences*, *7*, 301–313.

Matheny, A. M., Bohrer, G., Vogel, C. S., Morin, T. H., He, L., Prata de Moraes Frasson, R., et al. (2014). Species-specific transpiration responses to intermediate disturbance in a northern hardwood forest. *Journal of Geophysical Research: Biogeosciences*, *119*, 2292–2311. https://doi.org/10.1002/2014JG002804

Meyers, T. P., & Hollinger, S. E. (2004). An assessment of storage terms in the surface energy balance of maize and soybean. *Agricultural and Forest Meteorology*, *125*, 105–115.

Monson, R. K., Turnipseed, A. A., Sparks, J. P., Harley, P. C., Scott-Denton, L. E., Sparks, K., & Huxman, T. E. (2002). Carbon sequestration in a high-elevation, subalpine forest. *Global Change Biology*, *8*, 459–478.

Niu, G.-Y., Yang, Z.-L., Mitchell, K. E., Chen, F., Ek, M. B., Barlage, M., et al. (2011). The community Noah land surface model with multiparameterization options (Noah-MP): 1. Model description and evaluation with local-scale measurements. *Journal of Geophysical Research*, *116*, D12109. https://doi.org/10.1029/2010JD015139

Oleson, K. W., Lawrence, D. M., Bonan, G. B., Drewniak, B., Huang, M., Koven, C. D., et al. (2013). *Technical description of version 4.5 of the community land model (CLM)*, NCAR Technical Note NCAR/TN-503+STR. Boulder, CO: National Center for Atmospheric Research. https://doi.org/10.5065/D6RR1W7M

Pahlow, M., Parlange, M. B., & Port-Agel, F. (2001). On Monin-Obukhov similarity in the stable atmospheric boundary layer. *Boundary-Layer Meteorology*, *99*, 225–248. https://doi.org/10.1023/A:1018909000098

Stoy, P., Mauder, M., Foken, T., Marcolla, B., Boegh, E., Ibrom, A., et al. (2013). A data-driven analysis of energy balance closure across FLUXNET research sites: The role of landscape scale heterogeneity. *Agricultural and Forest Meteorology*, *171-172*, 137–152. https://doi.org/10.1016/j.agrformet.2012.11.004

Turnipseed, A. A., Blanken, P. D., Anderson, D. E., & Monson, R. K. (2002). Energy budget above a high-elevation subalpine forest in complex topography. *Agricultural and Forest Meteorology*, *110*(3), 177–201. https://doi.org/10.1016/S0168-1923(01)00290-8

Zhang, G., Leclerc, M. Y., & Karipot, A. (2010). Local flux-profile relationships of wind speed and temperature in a canopy layer in atmospheric stable conditions. *Biogeosciences*, *7*, 3625–3636. https://doi.org/10.5194/bg-7-3625-2010

Zheng, W., Ek, M., Mitchell, K., Wei, H., & Meng, J. (2017). Improving the stable surface layer in the NCEP Global Forecast System. *Monthly Weather Review*, *145*(10), 3969–3987. https://doi.org/10.1175/MWR-D-16-0438.1